DOI: 10.1017/S1431927605507669
Microsc Microanal 11(Suppl 2), 2005

Multifocal Three-Dimensional Imaging with Optical Lattice Excitation

Eric Betzig

New Millennium Research, LLC, 2174 Butternut Dr., Okemos, MI 48864

Two new classes of optical lattices have been identified [1] that permit the creation of arbitrarily large three-dimensional (3D) arrays of tightly confined excitation maxima of controllable periodicity and polarization from the superposition of a finite set of plane waves (e.g., Fig. 1). Such lattices can serve as 3D multifocal excitation fields for massively parallel fluorescence imaging within living cells, and may prove to be key enablers for the practical adaptation of superresolution techniques [2,3] to intracellular research.

A method for the generation of such lattices over an excitation zone of controllable extent has been devised [4], involving a combination of localized illumination at specific points in the rear pupils of opposed high numerical aperture (NA) microscope objectives with additional beams external to the objectives created with individual low NA lenses (Fig. 2). This geometry allows for efficient, simultaneous, and individualized detection of luminescence from a plurality of excitation maxima across multiple lattice planes when used in conjunction with appropriate spatial filtering aperture arrays and phase shift masks to compensate for differing degrees of spherical aberration in different lattice planes.

Diffraction calculations indicate that the effective excitation point spread function (PSF_{exc}) of the maxima created by these means is superior (Fig. 3) to that obtained in confocal microscopy and, due to the inclusion of the external beams, does not exhibit the side lobes characteristic of 4Pi excitation [5]. Furthermore, because the lattice periodicity is divorced from the excitation confinement, easily resolvable, highly confined maxima can be created in 2D by applying lattice excitation to total internal reflection (TIR) microscopy with high index ($n > 2$) substrates. Lattices of excitation nodes surrounded by spherical excitation shells can also be created, serving as depletion lattices for multifocal stimulated emission depletion (STED) microscopy [3] with improved effective PSF_{exc} .

Imaging simulations on an idealized network of fluorescent filaments (Fig. 4) further indicate the superior imaging capabilities of lattice excitation for standard 3D fluorescence imaging, as well as the resolution gains that may be achieved by the adaptation of TIR or STED methods. Unlike widefield and confocal microscopy, where out-of-plane excitation leads to undesirable background (only partially alleviated by pinhole filtering) and inefficient use of the photobleaching-mandated photon budget within the specimen, the constructive interference at the lattice maxima and partial destructive interference at other points leads to significantly greater molecular sensitivity and efficiency in converting any emitted photons into usable signal.

References

[1] E. Betzig, submitted to *Phys. Rev. Lett*.
[2] G. Cragg and P.T.C. So, *Opt. Lett.* 25 (2000) 46.
[3] M. Dyba and S.W. Hell, *Phys. Rev. Lett.* 88 (2002) 163901.
[4] E. Betzig, submitted to *Opt. Express*.
[5] S. Hell and E.H.K. Stelzer, *J. Opt. Soc. Am.* A9 (1992) 2159.

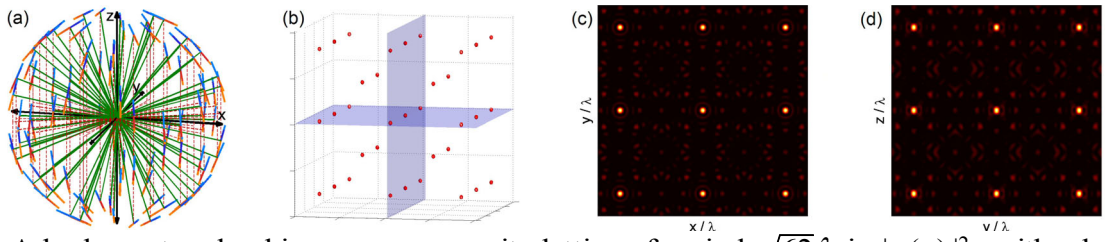

Fig. 1. A body-centered cubic sparse composite lattice of period $\sqrt{62}\lambda$ in $|\mathbf{e}(\mathbf{x})|^2$, with a basis that optimizes $|\mathbf{e}(\mathbf{x})\cdot\hat{\mathbf{e}}_z|^2$ at the excitation maxima: (a) wavevectors (green) and electric field vectors (multiple colors) at different times for the 96 plane waves comprising the lattice; (b) isosurfaces of $0.5\max[|\mathbf{e}(\mathbf{x})|^2]$ over $(10\lambda)^3$; (c,d) plots of $|\mathbf{e}(\mathbf{x})|^2$ in the *xy* and *yz* planes shown in (b), indicating high confinement of the excitation with good contrast relative to the remainder of each primitive cell.

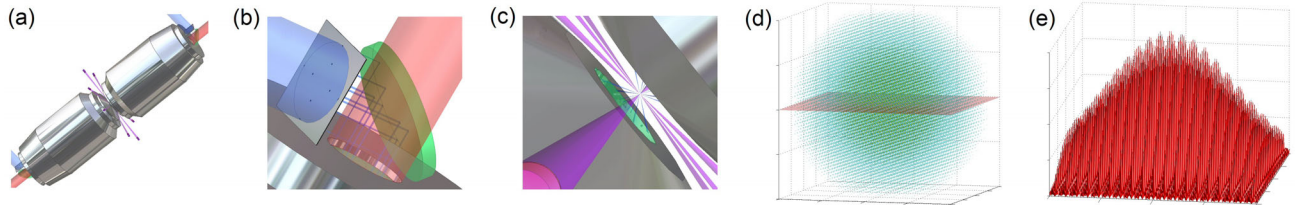

Fig. 2. Hybrid excitation of a bound lattice: (a) overall view, showing opposed objectives; (b) expanded view near one rear pupil, showing input beams (blue) defined with an aperture mask, and an output signal beam (red) isolated with a dichroic mirror (green); (c) expanded view between the objectives, showing 8 convergent beams (blue) generated internal to each objective as well as 8 beams (purple) generated externally with individual low NA lenses; (d) Resulting lattice over $(21\lambda)^3$, exhibiting a spherical excitation zone; (e) plot of $|\mathbf{e}(\mathbf{x})|^2$ in the *xy* plane shown in (d).

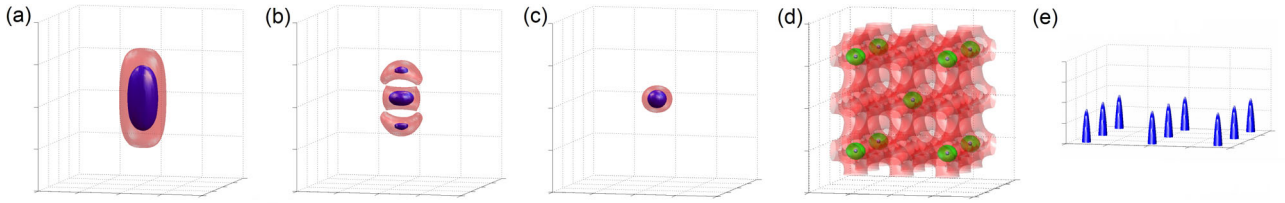

Figs. 3a,b. Isosurfaces of 50% (blue) and 16% (translucent red) of $\max[|\mathbf{e}(\mathbf{x})|^2]$ for (a) confocal and (b) 4Pi excitation at $NA = 1.2$ and $n = 1.33$. (c) Similar isosurfaces for a lattice excitation maximum created by the means shown in Fig. 2. (d) Excitation (translucent green), depletion (translucent red), and resulting effective excitation (blue) in STED lattice microscopy. (a-d) are plotted over $(\pm 2\lambda)^3$. (e) Isosurfaces of $0.5\max[|\mathbf{e}(\mathbf{x})|^2]$ over $\pm 2\lambda \times \pm 2\lambda \times 0.1\lambda$ for lattice TIR excitation at a GaN ($n = 2.45$) / water interface.

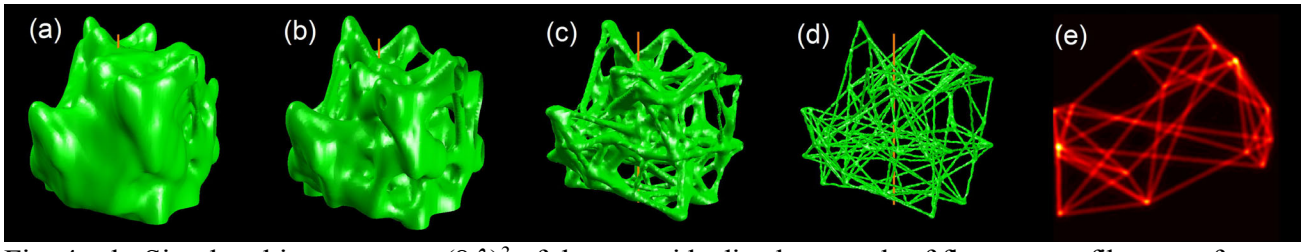

Fig. 4a-d. Simulated images over $(8\lambda)^3$ of the same idealized network of fluorescent filaments for: (a) widefield; (b) confocal; (c) linear lattice; and (d) lattice STED microscopy. (e) 2D simulation of lattice TIR microscopy over $(8\lambda)^2$ at a GaP ($n = 3.4$) / water interface.

https://doi.org/10.1017/S1431927605507669 Published online by Cambridge University Press